Comparison of Responses of a MMC Using Classical and Unified Constitutive Matrix Behaviors

J.L. Kroupa[1], J.A. Sherwood[2], N.E. Ashbaugh[1],
H.M. Quimby[2], and M.J. Boyle[1]

[1]University of Dayton Research Institute
Dayton, Ohio 45469

[2]University of New Hampshire
Durham, New Hampshire 03824

Abstract

Unified inelastic strain theories have been developed to characterize nonlinear material response with different physical-phenomena bases than previously used 'classical' treatments of plastic and creep strains. An enhanced understanding of these plasticity theories and their applications has been developed by the comparison of their resulting stress/strain response when applied to a titanium matrix composite subjected to thermal and mechanical loadings. Various baseline thermal, mechanical, and thermomechanical load scenarios were chosen to demonstrate the various features of the unified inelastic strain and classical constitutive theories. The basic underlying physical phenomena, numerical efficiencies and results from the scenarios are discussed for both theories.

Introduction

Titanium matrix composites will be exposed to such extreme thermal and mechanical load conditions that the matrix material will experience both plastic and time dependent deformation. Accurate representation of this nonlinear material behavior is essential for realistic determination of stress/strain response and life predictions. To model the matrix behavior in these extreme thermal and mechanical conditions, a unified inelastic strain theory has been employed in an attempt to describe the material's response more accurately than can be done with a 'classical' treatment of plastic and creep strains. The refined accuracy of unified theory is due to additional physical interpretations not found in classical theories. The resulting stress/strain response from the unified strain theory was compared against classical theory results in order to evaluate the performance of these two theories in titanium aluminide matrix composite applications. The response was determined from a commonly assumed axisymmetric composite geometry with load conditions representative of those found in laboratory conditions. The comparison also considered similarities and differences in theoretical derivation.

Historically, classical plasticity theories date back to 1864 when Tresca developed a yield criterion. St. Venant, Von Mises, Prandel, Reuss and others later enhanced the description of classical plasticity [1]. The physical phenomena of creep and associated descriptions of dislocation movement were recognized in the 1950's [2]. The 1970's marked an increase in numerical applications of the elastic-plastic-creep theories with the advent of finite element analysis [3]. The unified inelastic strain concept used in this study was based on the Bodner/Partom relationships, published in 1975 [4], developed to characterize strain rate dependent materials. Later, Stouffer and Ramaswamy [5,6] employed a similar form of the unified strain theory with the addition of 'back stress' to capture directional hardening and strain recovery phenomena at room and elevated temperatures. This current variety of unified strain theory was implemented into the finite element package ADINA by Sherwood [7]. The present paper compares Sherwood's form of unified theory with the classical elastic-plastic-creep derivation currently available with ADINA.

Theoretical Review

The basic equations of the classical and unified theories are reviewed in this section. Some major assumptions and rules to be reviewed include the decomposition of total strains, a Von-Mises yield criterion, flow rules and inelastic-strain evolution equations. Additional details of the unified strain theory are presented by Stouffer and Ramamamy [5,6]. The description of the implementation of the classical elastic-plastic-creep model in ADINA is given by Bathe [8,9].

The first assumption of a unified constitutive theory is that the total strain, ε^{tot}, can be decomposed into elastic, ε^{el}, thermal, ε^{th}, and inelastic strains, ε^{in}. Thus, the strain compatibility equations is written as

$$\varepsilon_{ij}^{tot} = \varepsilon_{ij}^{el} + \varepsilon_{ij}^{th} + \varepsilon_{ij}^{in}. \qquad \text{eq. (1a)}$$

The classical model further decomposes the inelastic strains into plastic, ε^{pl}, and creep, ε^{cr} ,components such that the strain compatibility equations become

$$\varepsilon_{ij}^{tot} = \varepsilon_{ij}^{el} + \varepsilon_{ij}^{th} + \varepsilon_{ij}^{pl} + \varepsilon_{ij}^{cr}. \qquad \text{eq. (1b)}$$

This uncoupling of the inelastic strains is somewhat physically unrealistic, as it is experimentally difficult to isolate plastic and time-dependent motion of dislocations.

The description of plastic deformation and directions of plastic flow in classical theory uses the Von-Mises yield criterion as given by

$$F = \frac{3}{2}(s_{ij} - \alpha_{ij})(s_{ij} - \alpha_{ij}) - k^2 = 0, \qquad \text{eq. (2)}$$

where F is the yield function, s_{ij} are components of the deviatoric stress, α_{ij} are components of directional hardening, and k is the uniaxial yield surface.

Plastic flow occurs when the stress state intercepts the yield surface, F, and loading continues outward and normal to the surface. The resulting direction of incremental plastic flow coincides with the outward normal to the yield surface. Thus, the classical plastic flow rule is written as

$$\dot{\varepsilon}_{ij}^{pl} = \lambda \frac{\partial F}{\partial \sigma_{ij}}, \qquad \text{eq. (3)}$$

where λ is a scaling factor. For the Von Mises yield surface, the flow rule reduces to

$$\dot{\varepsilon}_{ij}^{pl} = \lambda\, 3(s_{ij} - \alpha_{ij}). \qquad \text{eq. (4a)}$$

In contrast to the classical theory, the unified strain theory has no yield criterion, however inelastic flow rate is assumed as

$$\dot{\varepsilon}_{ij}^{in} = \lambda\, (s_{ij} - \Omega_{ij}), \qquad \text{eq. (4b)}$$

where λ is the scaling factor and Ω_{ij} are components of back stress. Thus, the direction of incremental inelastic strain is parallel to $s_{ij} - \Omega_{ij}$.

The classical theory defines an additional flow rule to describe the direction and magnitude of the incremental creep strain as

$$\dot{\varepsilon}_{ij}^{cr} = \mu\,(s_{ij} - \alpha_{ij}), \qquad \text{eq. (4c)}$$

where μ is a scaling factor.

Both theories describe the evolution of inelastic strain in a one-dimensional or an effective-strain sense. The classical evolution equation for differential isothermal effective plastic strain is described with an effective stress and a hardening factor H:

$$\dot{\varepsilon}_{eff}^{pl} = \frac{2}{3H}\dot{\sigma}_{eff}, \qquad \text{eq. (5a)}$$

where $\sigma_{eff} = \sqrt{3J_2} = \sqrt{3(s_{ij})(s_{ij})/2}$,

and H is a function of the elastic and plastic moduli. Addition thermal differential terms of the elastic and plastic moduli are not shown here for simplicity. For this analysis, the classical model assumes isotropic hardening, thus $\alpha_{ij}=0$. This classical evolution equation for plastic strain is derived from empirical relationships within stress/strain behavior with little regard to the physics governing hardening behavior.

With a more physical basis than the classical derivations, inelastic-strain evolution equations for unified theory describe the kinematics of slip planes in the presence of dislocation pile-ups. The inelastic-strain evolution equation takes the form

$$\dot{\varepsilon}_{eff}^{in} = D_0 \exp\left[\frac{-1}{2}\left\{\frac{Z}{\sqrt{3K_2}}\right\}^{2n}\right], \qquad \text{eq. (5b)}$$

where $3K_2 = 3(s_{ij} - \Omega_{ij})(s_{ij} - \Omega_{ij})/2$,

D_0 is a limiting strain rate, and Z is the drag stress. The drag stress accounts for temperature-dependent isotropic hardening and evolves with plastic work. For this study, the drag stress remains constant with respect to plastic work and is set to its initial isothermal value of Z_0. The evolution of back stress is given as

$$\dot{\Omega}_{ij} = f_3\dot{s}_{ij} + \dot{f}_3 s_{ij} + f_1\dot{\varepsilon}_{ij}^{in} - \frac{2}{3}f_1\left(\frac{\Omega_{ij}}{\Omega_{sat}}\right)\dot{\varepsilon}_{eff}^{in}, \qquad \text{eq. (5c)}$$

where f_1 and f_3 are material constants. This back stress accounts for kinematric hardening. The saturation value for the back stress, Ω_{sat}, is a time and temperature dependent limiting value of back stress evolution. The saturated back stress evolution equation is written as

$$\dot{\Omega}_{stat} = -\hat{B}\left|\frac{\sqrt{3J_2}}{\sigma_0}\right|^r (\Omega_{stat} - \Omega_{cr}), \qquad \text{eq. (6a)}$$

where $\hat{B}$, r and Ω_{cr} are material constants and σ_0 is a normalization factor.

The equation for the classical creep model is assumed as

$$\varepsilon^{cr}_{eff} = a_0 \sigma^{a_1}_{eff} \{t^{a_2} + a_3 t^{a_4} + a_5 t^{a_6}\} \exp\left[\frac{a_7}{\theta}\right], \qquad \text{eq. 6b}$$

where a_0, a_1, a_2, a_3, a_4, a_5, a_6 and a_7 are material constants and θ is the current temperature in degrees Kelvin. Within this creep model, the exponent term for the temperature dependence is physically based on the activation energy of dislocation motion. The remaining constants are determined from best fit of experimental results, with little physical basis.

Summarizing the constitutive equations for the two theories, the classical model contains 13 material constants, while the unified model contains 14 material constants. Unified strain theories contain additional physical basis, such as the coupling of plastic and time-dependent strains and an elegant form for the kinematics of inelastic strain as prescribed by dislocation motion. Both models were incorporated into the finite element package ADINA. The classical theory is part of the standard ADINA software package, while the unified strain model has been implemented in the form of user subroutines by Sherwood [7].

Composite Modeling and Material Properties

The axisymmetric representation of unidirectional silicon carbide fibers reinforcing a titanium aluminide matrix comprised the composite model. Preliminary results from longitudinal loadings of unidirectional composites with a more complex three-dimensional unit cell model revealed a stress state which was essentially axisymmetric. Thus, the axisymmetric geometry was quite suitable for this analysis. The fiber volume content was 0.35 which is typical of many currently fabricated titanium aluminide composites. Four 8-noded axisymmetric elements represented the fiber and eight elements modeled the matrix, as shown in Figure 1. The boundary conditions shown were designed to give zero radial/axial shear stress throughout the composite, uniform axial strain and zero radial stress at the outer radius of the matrix (r_{max}). The matrix stress was investigated at two critical locations - at the fiber-matrix interface (pt A) and at the outer radius of the matrix (pt B).

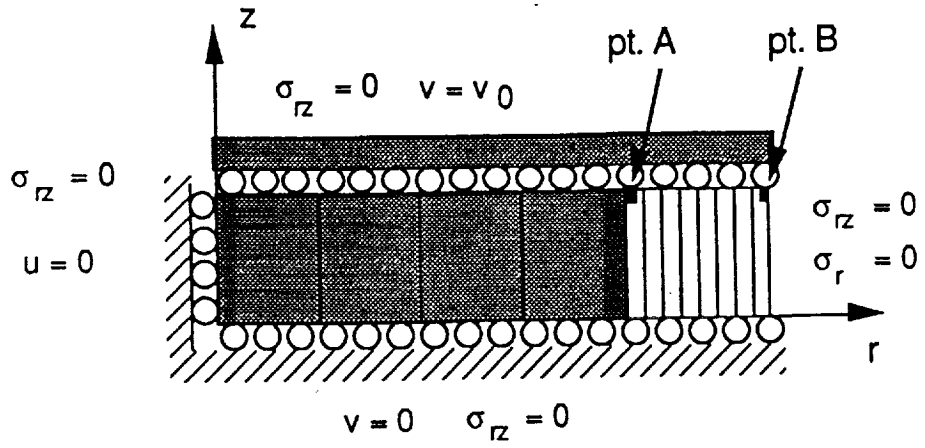

Figure 1 Axisymmetric Representation of the Composite.

Uniaxial material properties of the Ti-24Al-11Nb matrix were obtained from fiberless material processed in the same manner as the composite. The process consisted of plasma spraying fiberless foils, laying up the foils in panels and hot isostatically pressing the panels [10]. This processing technique was selected to closely match matrix-material texture and microstructure as found in the consolidated composite. These panels were experimentally tested at a variety of temperatures to obtain the uniaxial stress/strain response and coefficients of thermal expansion.

A bilinear stress/strain response, with the associated material constants for the Ti-24Al-11Nb matrix given in Table 1, was assumed for the classical model. Material properties for the unified model, given in Table 2, were determined from the same Ti-24Al-11Nb stress/strain response as used in the classical model. The creep constants are representative of bulk Ti-24Al-11Nb, as the constants were derived from a limited amount of creep data of a forged plate rather than of the plasma sprayed stock. For consistency, both constitutive theories determined their own material constants from the same creep response data. The fiber response was assumed to be linear elastic, with material constants given in Table 3.

6.

Table 1

Ti-24Al-11Nb Material Constants for Classical Model [10]

$\upsilon = 0.3$

Temperature (°C)	Elastic Modulus (GPa)	Yield Strength (MPa)	Plastic Modulus (GPa)	Secant CTE (10^{-6}/°C) T_{ref} = 950 °C
21.0	94.0	604.0	1.130	12.19
93.0	92.0	572.0	0.700	12.39
204.0	91.0	498.0	0.719	12.77
316.0	89.0	447.8	0.692	13.24
427.0	79.0	421.0	0.415	13.79
538.0	72.5	379.5	1.360	14.43
649.0	49.5	351.0	0.479	15.15
760.0	30.5	248.5	0.584	15.95
871.0	16.0	155.0	0.217	16.84
982.0	12.1	40.0	1.180	17.84

Creep Constants for Eq. (6b)

$a_0 = 1.123 \times 10^{-4}$ $a_1 = 2.4018$ $a_2 = 0.5746$

$a_3 = 0$ $a_4 = 0$ $a_5 = 0$

$a_6 = 0$ $a_7 = 14195$ (Units: MPa, K, s)

Table 2

Ti-24Al-11Nb Material Constants for Unified Strain Model [7]

$D_0 = 1.\times 10^4$, $\upsilon = 0.3$

T (°C)	CTE (10^{-6}/ C°) T_{ref} = 950 °C	n	Z_0	E (GPa)	f_1 (10^3)	f_3	Ω_{sat} (MPa)
21.	12.31	1.30	484.	94.065	144.38	0.7926	317.33
93.	12.35	1.30	484.	91.328	65.317	0.7800	290.00
204.	12.39	1.25	491.	88.817	36.437	0.7665	251.33
316.	12.71	1.12	517.	89.328	55.000	0.7740	227.33
427.	13.25	1.00	551.	73.165	68.750	0.7680	218.00
538.	13.99	0.87	970.	70.333	78.385	0.6572	186.67
649.	14.94	0.70	1649.	44.035	88.000	0.5000	142.67
760.	16.11	0.52	4384.	25.012	17.187	0.3500	82.00
871.	17.48	0.30	49012.	18.953	7.562	0.0010	16.67
982.	19.05	0.15	5.0×10^6	18.000	4.000	0.0001	12.00

Creep Constants for Eq. (6a) at 650 °C

$\hat{B} = 4.55 \times 10^{-8}$ $r = 2.0853$ $\Omega_{cr} = 29.33$ MPa

$\Omega_{hi} = 351.00$ MPa $\Omega_{low} = 100.0$ MPa

Table 3

SCS-6 Material Constants for Linear Elastic Model [10]

E = 414.0 GPa, υ = 0.3

Temperature (°C)	Secant CTE (10^{-6}/°C), T_{ref} = 950 °C
20.0	4.65
101.0	4.75
203.0	4.91
299.0	5.04
400.0	5.18
500.0	5.32
598.0	5.39
702.0	5.46
800.0	5.64
900.0	5.79
1001.0	5.67

Results

The axisymmetric representation of the composite was subjected to a number of typical thermal and mechanical load scenarios as found in the laboratory. The four load cases considered were initial cooling following the consolidation process, out-of-phase thermal mechanical fatigue, sustained loading at 650°C and residual stress "shake-down" during thermal cycling. Since the unified-strain-theory material constants for creep were only determined for 650°C, use of the classical transient-temperature creep model (eq.6b) and unified strain's creep model (eq.6a) was restricted to the sustained load scenario. A comparison of the CPU time usage for each scenario was conducted to evaluate the numerical performance of the classical and unified-strain models.

Thermal Processing

Residual stress from processing effects the composite response during subsequent thermal or mechanical loading. The state of residual stress due to thermal processing was determined using both the classical and unified theories for the matrix behavior. Since the creep constants at a variety of temperatures were not available for the unified strain model, the thermal processing results were determined in the absence of the classical and unified strain's creep models (a_0 =0 and $\hat{B}$=0).

The simulation of cooling after thermal processing considered an initial zero stress/strain state at 950°C (t_0=0) followed by composite cooling to room temperature in one hour, (t_1=3600s) The predicted residual matrix stress state at

the fiber-matrix interface (pt. A) during the cooling process compared quite well for both models, as illustrated in Figure 2. As a better measure of comparison, the inelastic strains were investigated and also revealed reasonable agreement, illustrated in Figure 3. The initial growth of appreciable plastic strains occurred at 550°C for both models, thus demonstrating that the unified strain theory predicted the same thermal elastic solution above 550°C as determined by the classical theory. Below 550°C, the classical solution proceeded in such a manner that the effective stress remained on the temperature dependent yield surface. A similar 'stress limiting' phenomenon occurred in the unified strain theory, as the back stress reached its temperature dependent saturated value and remained in the saturated state for the remaining segment of cooling.

The unified model's ability to characterize rate-dependent-loading effects was demonstrated by conducting the residual stress scenario at three different cooling rates: 36, 360 and 3600 seconds. The different cooling rates did effect the resulting effective stress ($\sqrt{3J_2}$) and the state variable $\sqrt{3K_2}$, but not to a great extent, as illustrated in Figure 4. This lack of significant strain-rate effect on matrix response may be due to an inadequate amount of experimental data which characterized the strain-rate behavior of this material.

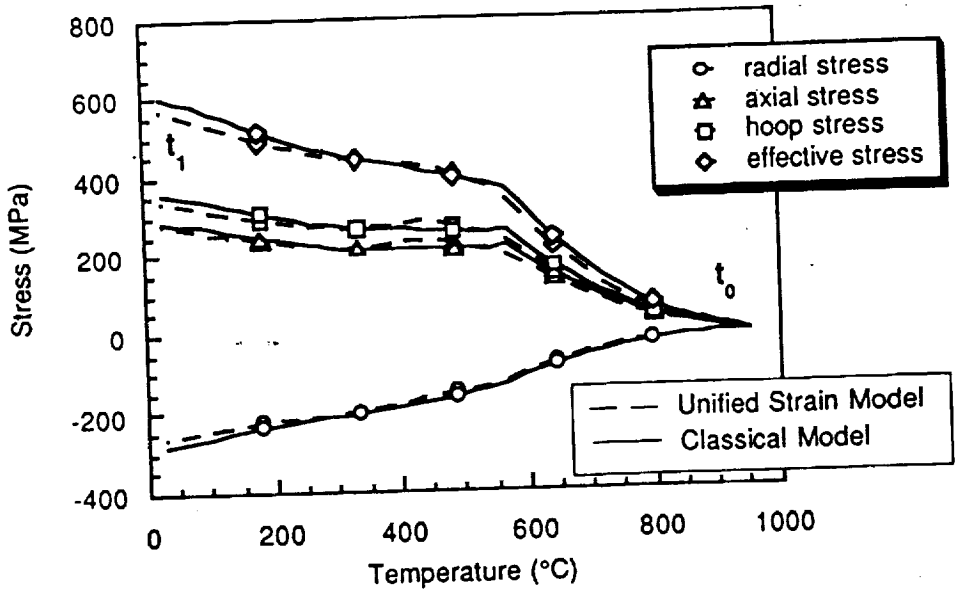

Figure 2 Processing Induced Residual Matrix Stress Predictions at Fiber-Matrix Interface (pt. A) for Unified Strain and Classical Models.

9

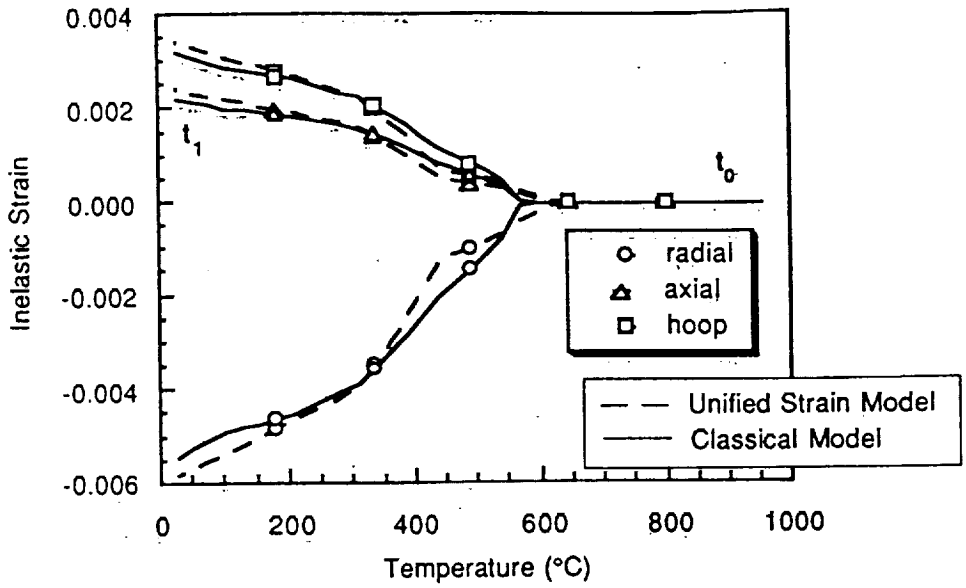

Figure 3 Processing Induced Residual Matrix Inelastic Strain at Fiber-Matrix Interface (pt. A) Predicted from Unified Strain and Classical Models

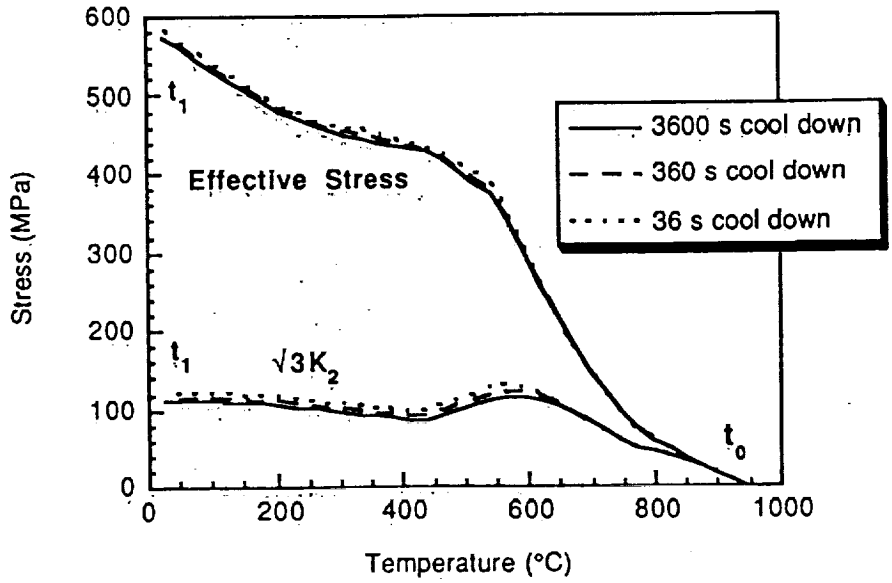

Figure 4 Matrix Effective Stress and State Variable $\sqrt{3}$K2 at Fiber-Matrix Interface (pt. A) Predicted From the Unified Strain Theory at Three Different Cooling Rates

Thermomechanical Loading

An out-of-phase thermomechanical fatigue load was considered for comparison of the two theories, since this combination of thermal and mechanical loads was more adverse on the matrix material than other TMF loadings. The TMF scenario, shown in Figure 5, began at the end of the thermal processing simulation (t1=3600s). The composite was then heated to 650°C, followed by the application of an aggregate axial load of 700 MPa. Within the finite element method the aggregate load was appropriately distributed throughout the entire composite to retain the uniform axial-strain condition. The temperature range of 150-650°C and stress range of 70-700 MPa were the same as those previously considered in TMF experiments conducted in the laboratory [11].

The resulting stress histories from both constitutive theories compared quite well at the matrix/fiber interface (pt. A), as illustrated in Figure 6. Throughout the entire loading scenario, the classical model did not exhibit fully-reversed yield behavior, since the yield surface and the effective stress failed to intercept each other at the peak load conditions. This was not expected, since it was hoped that any reversed plasticity and subsequent work hardening would be better displayed with the unified strain theory than with the classical theory. The unified theory exhibited strain ratcheting, but not fully reversed plasticity, as illustrated by the axial stress and mechanical strain response shown in Figure 7. The classical elastic-plastic theory with the absence of time dependent behavior did not predict any hysteresis or strain ratcheting, since stress levels remained in the elastic regime. The stability of the observed strain ratcheting was not investigated for the limited number of load cycles applied.

The stresses was also investigated at the outer radius of the matrix cylinder (pt. B), which exhibited a large axial stress component, as illustrated in Figure 8. Again, the stress state predicted by the two constitutive theories compared quite well at this location. However, the classical results still did not predict any reversed inelastic response. Instead, it was found that at 650°C the peak axial stress of 610 MPa exceeded the uniaxial yield strength of 540 MPa. In comparison, the peak axial stress at the fiber-matrix interface was 440 MPa. Similar to the findings at the fiber-matrix interface, the unified strain theory did predict axial strain ratcheting at the outer radius of the matrix, as illustrated in Figure 9. In a physical sense, from the larger axial stress at this location in the matrix (pt. B), accelerated damage and/or fatigue crack initiation would be more likely than at the fiber-matrix interface (pt. A).

11

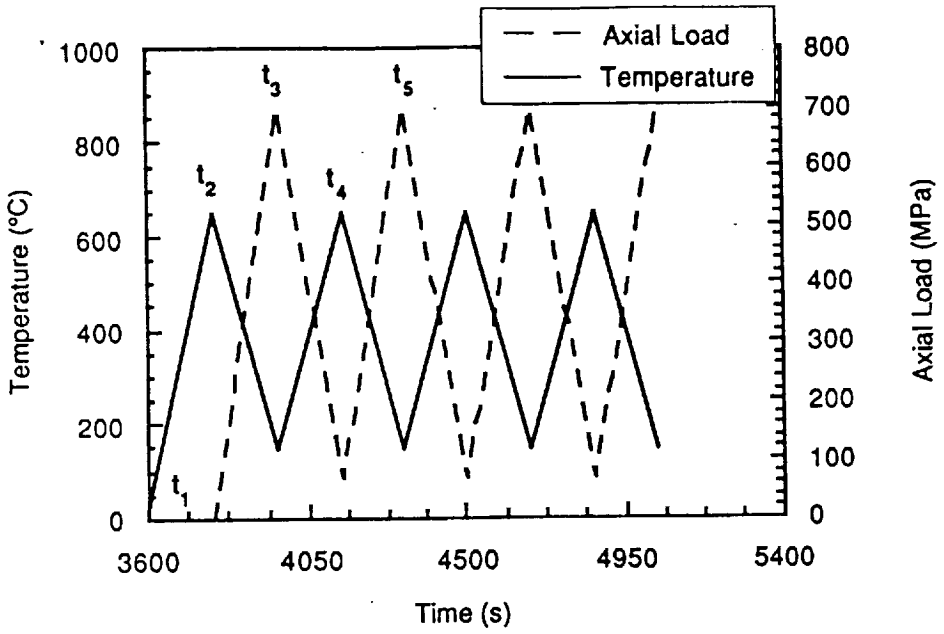

Figure 5 Loading Scenario for Out-of-Phase TMF Simulation.

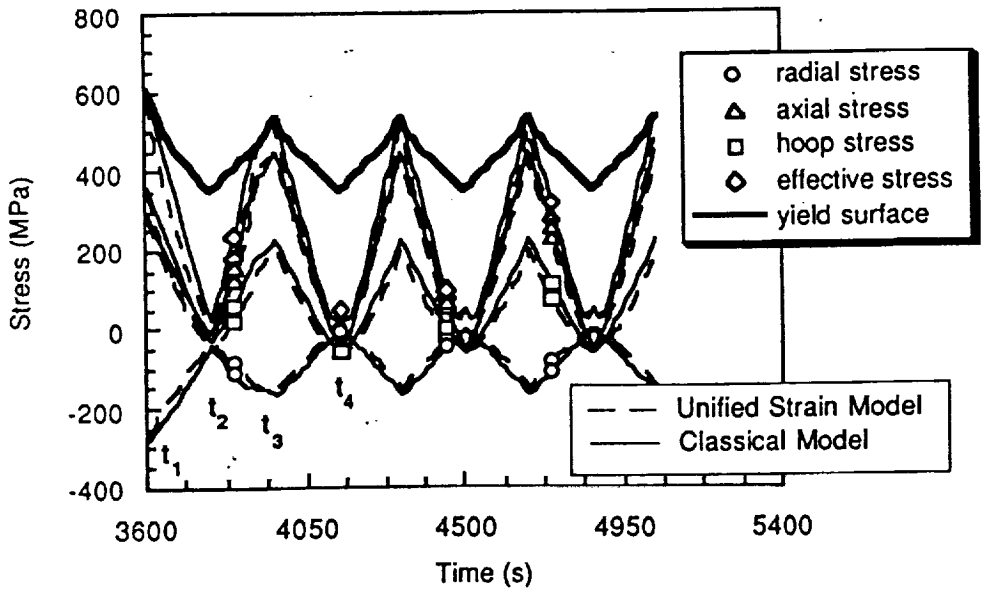

Figure 6 Predicted Matrix Stress Response at Fiber-Matrix Interface (pt. A) during Out-of-Phase TMF Loading.

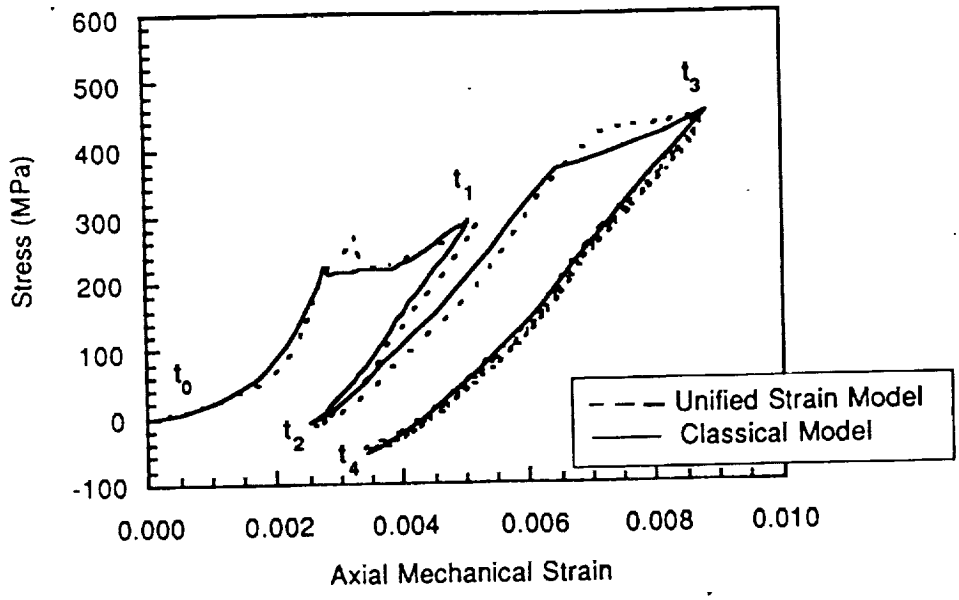

Figure 7 Axial Stress/Strain Response at Fiber-Matrix Interface (pt. A) during Out-of-Phase TMF Loading.

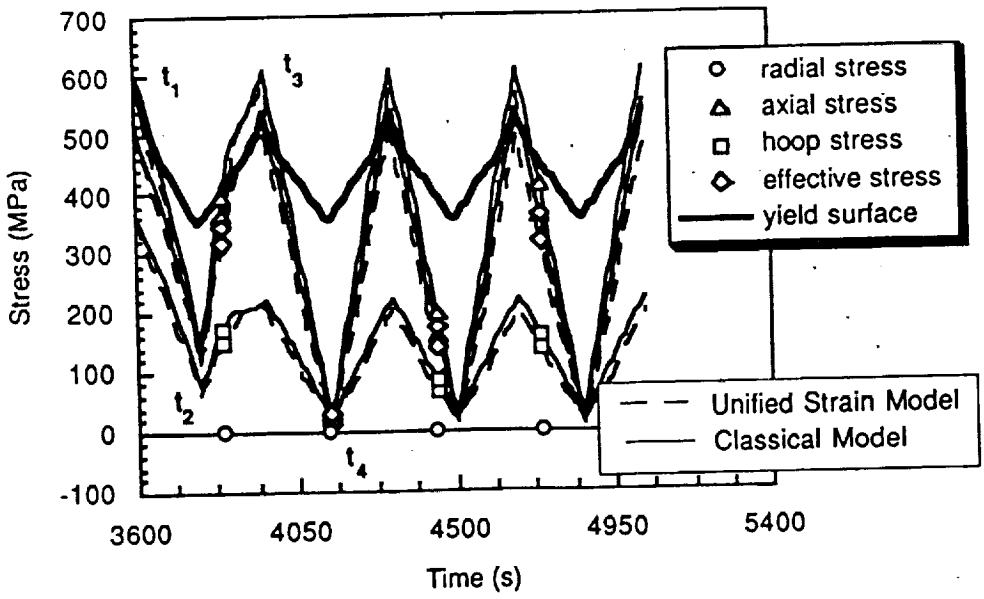

Figure 8 Predicted Matrix Stress Response at Outer Radius of Matrix (pt. B) During Out-of-Phase TMF Loading.

13

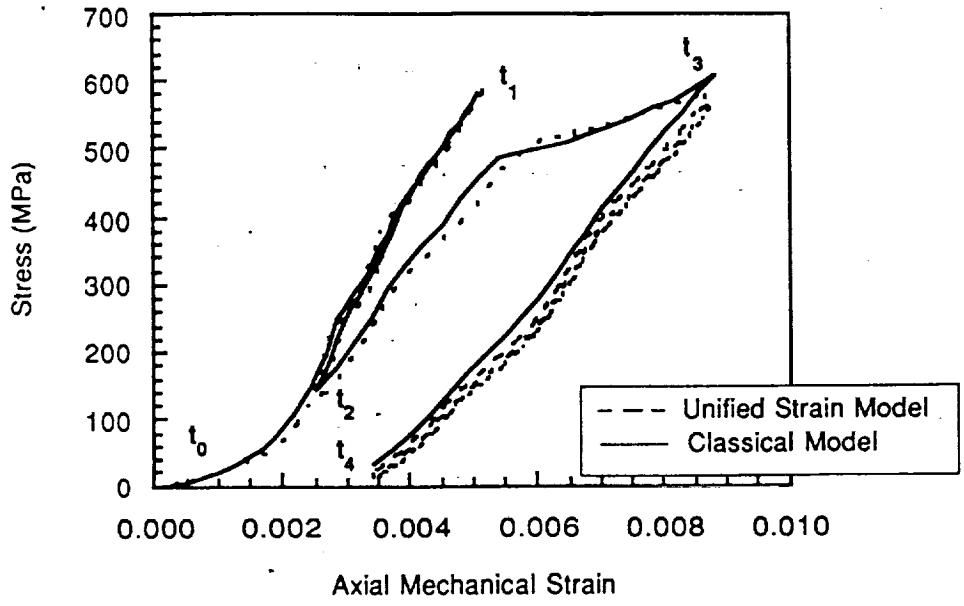

Figure 9 Axial Stress/Strain Response at Outer Radius of Matrix (pt. B) During Out-of-Phase TMF Loading.

Time Dependent Response

This load scenario was designed to demonstrate the time dependent response of the matrix predicted by both constitutive theories. The entire scenario consisted of thermal processing, heating the composite to 650°C, and application of a sustained axial load of 450 MPa for twenty hours. This load level and the hold time were representative of expected conditions of actual sustained load experiments conducted on composites. The load history shown in Figure 10 began at the end of the thermal processing simulation (t1=3600 seconds).

The time dependent response was best demonstrated by the axial stress at the outer radius of the matrix, as illustrated in Figure 11. Response from the two constitutive theories compared quite well during the cool down, t0-t1, heating to elevated temperature, t1-t2, and application of axial load, t2-t3. However, the two theories did not predict the same amount of stress relaxation during the hold time. This difference may be attributed to the lack of experimental creep data and the different stress extrapolation schemes between the two models.

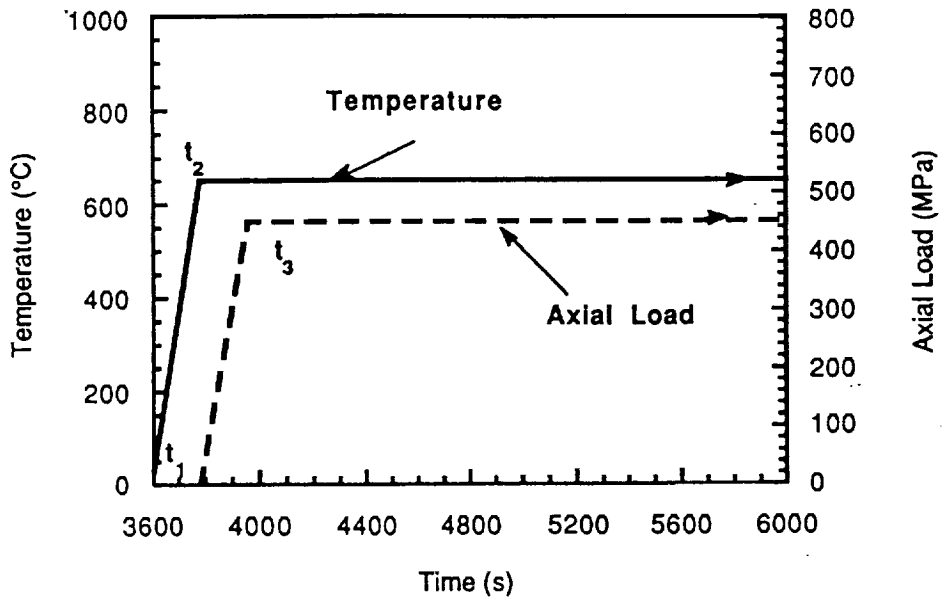

Figure 10 Load Scenario for Sustained Loading Simulation.

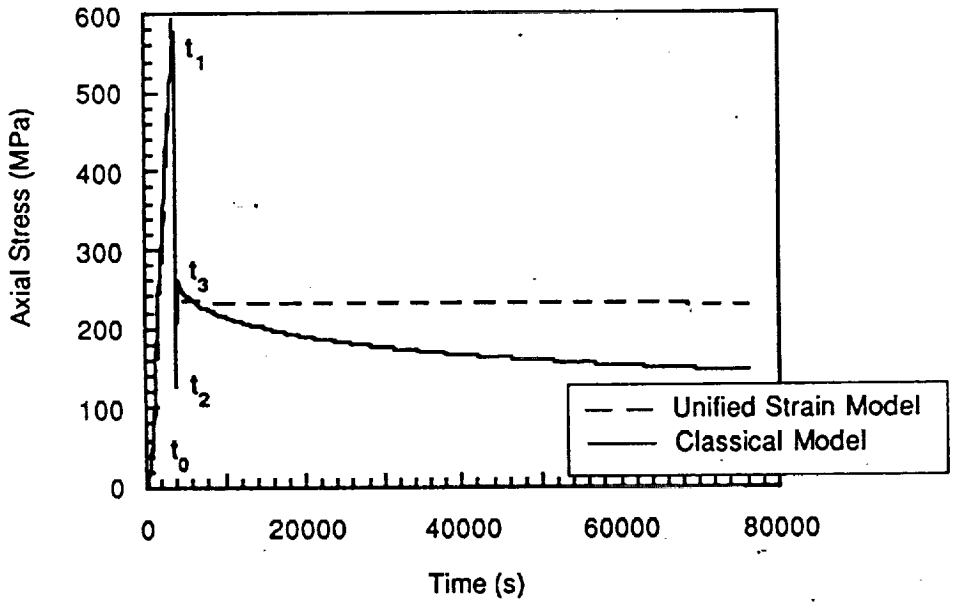

Figure 11 Axial Stress Prediction at Outer Radius of Matrix (pt. B) During Sustained-Loading Simulation.

Thermal Shakedown

Experimental investigations by James [12] have shown that the room temperature residual stress in the composite ratchets down for repeated thermal cycling between 65°C and 815°C. To analytically investigate this phenomenon, the composite model was cooled from its consolidation temperature of 950 °C to room temperature (25°C) and then subjected to 25 complete thermal cycles between 25°C and 950°C. The effective stress response of the matrix at the fiber-matrix interface (pt. A) for the classical and unified models are given Figure 12. The classical model without a time dependent behavior (a_0=0) does not predict the experimentally observed reduction in room temperature residual stress due to thermal cycling. However, the unified model shows a significant relaxation of stress level with this subsequent cycling. Use of the creep equation (Eq. 6b) in the classical theory may predict this 'shakedown' phenomenon, however the lack of high temperature creep data for the matrix prohibited its accurate use.

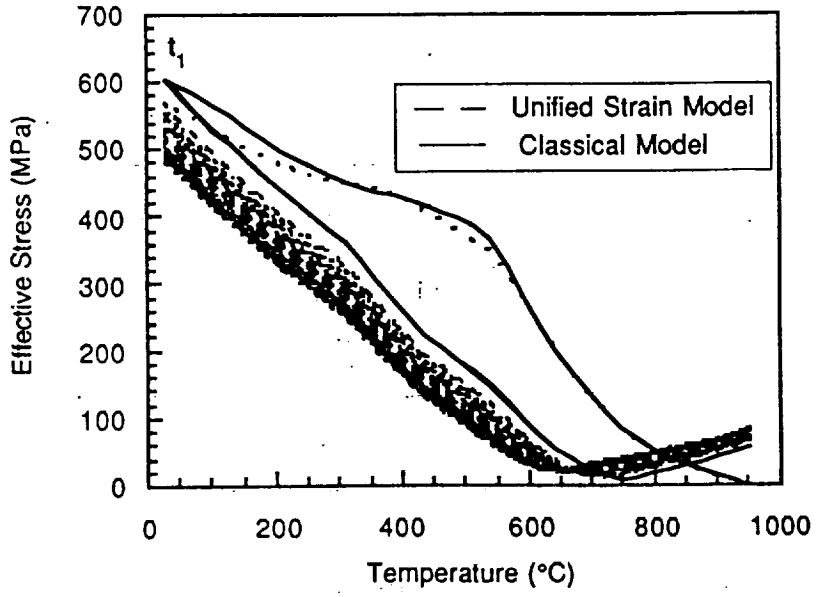

Figure 12 Predicted Matrix Effective-Stress Ratcheting During Thermal Shake-Down Loading.at Fiber-Matrix Interface (pt. A)

Computational Efficiency

The resulting CPU times for each analysis are compared to evaluate the numerical performance of the two models and numerical implementation. Numerical algorithms by Bathe [9] have made the classical model rather computationally efficient, while the unified strain models are notoriously CPU inefficient. The unified strain model's CPU inefficiency is due to the mathematical stiffness of its constitutive equations. By use of a relaxation factor and sub-

incremental solution increments, the efficiency ratio of the unified strain model over the classical model CPU usage has been reduced from an excessive factor of ten to a factor of roughly two to four times as summarized in Table 4. These results were dependent on hardware and associated compiler software. Since the numerical algorithms of the unified strain theory are still quite new, they are not expected to perform as well.

Table 4

Comparison of CPU Usage

Load Case	Constitutive Model	Number of Solution Increments	Number of Sub-Increments	CPU Seconds SUN*	CPU seconds IBM**
Residual Stress	Unified Strain	36	10	424.80	91.64
			1	-----	37.92
	Classical	36	1	69.37	48.25
TMF	Unified Strain	200	10	2141.8	402.57
			4	-----	272.87
	Classical	200	1	335.90	248.70
Creep	Unified Strain	260	10	1570	440.97
			4	-----	318.72
	Classical	260	1	897.01	310.38
Shake-down	Unified Strain	1836	10	------	3383.15
	Classical	1836	1	------	1159.25

* ADINA6.0 on SUN-SPARC2, Model 4/75
** ADINA6.0 on IBM-RS/6000, Model 530

Summary and Conclusions

Using a unified strain theory to represent matrix behavior, matrix response was obtained for an SCS-6 silicon carbide/titanium aluminide, Ti-24Al-11Nb axisymmetric composite model subjected to a variety of thermal and mechanical load scenarios. This response was compared with results obtained with 'classical' elastic-plastic-creep theory representing the matrix behavior. In conducting this investigation, the underlying physics and numerical efficiencies of the two theories were compiled and presented with some revealing results.

Comparison of the development of the two theories revealed that the unified strain derivation contained additional physical basis not found in the classical theory. The coupling of plastic and time dependent strains into an inelastic strain is viewed as more realistic, since separation of these two phenomena is experimentally difficult. The inelastic-strain-rate equations of unified strain theory are based on observations of the kinematics of dislocation movement, whereas classical plastic-strain-rate are based on empirical constructs of elastic and plastic response. The thermal term for the classical-creep-evolution equation was based on a physical description of an the activation energy required for dislocation movement.

Comparison of the results from both theories employed to represent the matrix response of a composite show good correlation for the residual stress and the TMF loading scenarios. The results obtained for the hold time scenario did not compare as well, since the models extrapolated stress effects on creep response by different methods. The unified model did predict some cooling-rate dependence during the residual stress cool down and some strain ratcheting during the TMF loading, which were not found in classical elastic-plastic theories in the absence of time dependent behavior. The unified model also captured stress relaxation during thermal shakedown simulations. With adequate amounts of creep data, accurate use of classical creep equation may predict the strain ratcheting and/or stress relaxation not found in the classical model results. In retrospect, it was no great surprise that a good comparison of results was found, since both theories modeled the matrix thermal and mechanical response quite well.

The resulting CPU times for each analysis were compared and used to evaluate the numerical performance of the two models. The comparison revealed that the unified inelastic strain theory was less computationally efficient by roughly two to four times than the classical model. However, these results were highly scattered depending on hardware and associated software. In addition, numerical methods and implementation of the unified strain theory are still quite new and can not be expected to perform as efficiently.

The chosen uniaxial geometry and load levels were too restrictive to display the finer aspects of the unified strain theory. Such fine aspects include directional hardening, reversed plasticity, and strain-rate effects. The unidirectional geometry was inappropriate as the fiber dominated the majority of the axial response. The load levels were too conservative as they represented loadings of an early

generation of composite with an inherently higher population of processing defects that could not withstand a more aggressive environment. For further analysis, a matrix dominate geometry with a more aggressive environment may provide a better basis for comparison of these two models.

References

[1] Hill,R., The Mathematical Theory of Plasticit , Oxford Press, New York, 1960.

[2] Sharifi, P.,and Yates, D. N., "Nonlinear Thermo-Elastic-Plastic and Creep Analysis by the Finite-Element Method", AIAA Journal, Vol. 12, No 9, pp1210-1215, Sept 1974.

[3] Boyle, J.T. and Spence, J., Stress Analysis for Creep, Butterworths and Co., London, England, 1983.

[4] Bodner, S. R, and Partom Y., "Constitutive Equations for Elastic Viscoplastic Strain Hardening Materials", ASME Journal of Applied Mechanics, 42, pp. 385-389, 1975.

[5] Stouffer, D.C., Ramaswamy, V.G., Laflen, J.H., Van Stone, R.H., and Williams, R. "A Consitutive Model for the Inelastic Multiaxial Response of Rene'80 at 871 C and 982 C", Journal of Engineering Materials and Technology, Vol. 112, pp. 241-246, April 1990.

[6] Ramaswamy, V.G., Stouffer, D.C., and Laflen, J.H., "A Unified Constitutive Model for the Inelastic Uniaxial Response of Rene' 80 at Temperatures Between 538C and 982C," Journal of Engineering Materials and Technology, vol. 112, pp. 280-286, July 1990.

[7] Sherwood, J.A.,and Boyle, M.J.,"Investigation of the Thermomechanical Response of a Titanium Alluminide/Silicon Carbide Composite Using a Unified State Variable Model in ADINA., Computers & Structures, Vol. 40, No. 2, pp. 257-269, 1991.

[8] Kojic, M. and Bathe, K., "Thermo-Elastic-Plastic and Creep Analysis of Shell Structures," Computers & Structures Vol. 26, No. 1/2, pp 1509-1532, 1987.

[9] Kojic M. and Bathe K., "The 'Effective-Stress-Function' Algorithm for Thermo-Elasto-Plasticity and Creep," International Journal for Numerical Methods in Engineering, Vol 24, pp. 135-143, 1987.

[10] Titanium Aluminide Composites, Third interim report for contract F33657-86-C-2136 submitted by GE to Material Laboratory-Air Force Aeronautial Laboratories, Wright-Patterson AFB, OH, 45433.

[11] Russ, S.M., "Thermal Fatigue of Ti-24Al-11Nb/ SCS-6," Metall. Transactions, Vol. 21, pp. 1595-1602, April 1990.

[12] James, M.R., "Behavior of Residual Stresses During Fatigue of Metal Matrix Composites," Proceedings at the International Conference on Residual Stresses, Tokushima, Japan, July 1991.